PROCEEDINGS OF SCIENCE

ONLINE ICRC 2021
THE ASTROPARTICLE PHYSICS CONFERENCE
Berlin | Germany
37th International Cosmic Ray Conference
12–23 July 2021

Discovery of TXS 1515-273 at VHE gamma rays and modelling of its Spectral Energy Distribution

S. Loporchio,[a,*] E. Lindfors,[b] V. Fallah Ramazani,[b,c] F. D'Ammando,[d] A. Arbet Engels,[e] L. Di Venere,[a] F. Giordano,[a] A. Nabizadeh,[f] E. Bissaldi,[a] M. Orienti[d] and S. Cutini[g] on behalf of the *Fermi*-LAT and MAGIC Collaborations[†]

[a] *INFN MAGIC Group: INFN Sezione di Bari and Dipartimento Interateneo di Fisica dell'Università e del Politecnico di Bari,I-70125, Bari, Italy*

[b] *Finnish MAGIC Group: Finnish Centre for Astronomy with ESO, University of Turku,FI-20014 Turku, Finland*

[c] *Ruhr University Bochum, Universitätsstraße 150, D-44801 Bochum, Germany*

[d] *INAF - Istituto di Radioastronomia, I-40129 Bologna, Italy*

[e] *ETH Zürich,CH-8093 Zürich, Switzerland*

[f] *Department of Physics and Astronomy, University of Turku,FI-20014 Turku, Finland*

[g] *INFN Sezione di Perugia,I-06123 Perugia, Italy*

E-mail: serena.loporchio@ba.infn.it

In February 2019, a flaring state of the extreme blazar candidate TXS 1515–273 was registered by the *Fermi*-LAT, which triggered observations with the MAGIC telescopes and the X-ray satellites *Swift*, *XMM-Newton* and *NuStar*. The observations led to the discovery of the source at very-high-energy (VHE, 100 GeV $\leq E \leq$ 100 TeV) gamma-ray energies and the detection of short time scales of variability (∼1 h) in several X-ray bands. The analysis of the observed variability helped us to constrain the physical parameters of the emission region. Thanks to the high-quality X-ray data, the synchrotron peak location was determined. The source was classified as a high synchrotron peaked source during the flaring activity. We constructed the broadband spectral energy distribution from radio to TeV. We interpreted it assuming leptonic emission and taking into account the constraints from the X-ray variability. We tested two scenarios: a simple one-zone model and a two-component model. Both models were found to describe the data well from X-ray to VHE gamma ray, but the two-zone model allows for a more accurate modelling of the emission at radio and optical energies.

37th International Cosmic Ray Conference (ICRC 2021)
July 12th – 23rd, 2021
Online – Berlin, Germany

*Presenter

†a complete list of the MAGIC Collaboration authors can be found at the end of the proceedings

PoS(ICRC2021)801

1. Introduction

Blazars, which are jetted active galactic nuclei (AGNs) seen at small viewing angles, are the most numerous gamma-ray sources in the extragalactic sky. The spectral energy distribution (SED) of blazars exhibits a double-bumped structure. The first bump in the SED, peaking in the frequency range from infrared to X-rays, is usually interpreted as to synchrotron emission from ultra-relativistic electrons in the jet. The high-energy bump peaks above MeV energies and is commonly explained as due to inverse Compton (IC) scattering, possibly of the same electron population on their synchrotron emission (synchrotron self-Compton, SSC).

There are two subclasses of blazars: flat spectrum radio quasars and BL Lac objects. The peak frequency of the synchrotron bump in the SED leads to a further classification of blazars into low-, intermediate-, and high-frequency peaked sources (LSP, ISP and HSP, respectively [1]). Only a complete energy coverage from the radio to TeV energy range (multi-wavelength observations, MWL) allows for a proper understanding of the emission mechanisms. Moreover, given the variability of the objects, shown in different energy ranges, simultaneous observations are required.

Up to and including the Third *Fermi*-LAT Catalog [2], TXS 1515–273 had been classified as a blazar candidate of uncertain type [3]. Only in the Fourth Fermi Catalog [4] was it classified as a BL Lac object with a photon index $\simeq 2$. The redshift was also unknown until recently when the observations of [5, 6] determined it to be z=0.1285. The MAGIC telescopes observed TXS 1515–273 during February 2019 as a part of a MWL campaign organized after flaring activity in the high-energy gamma-ray band (HE, 0.5 MeV $\leq E \leq$ 100 GeV) was reported by the *Fermi*-LAT [7]. Quasi-simultaneous observations were carried out by the Siena observatory, the KVA telescope, the *Neil Gehrels Swift observatory*, the *XMM* observatory, the *NuSTAR* telescope and the MAGIC telescopes, while radio observations close in time to the MWL campaign were performed with the Very Long Baseline Array (VLBA) Experiment. The observations in the very-high-energy (VHE, 100 GeV $\leq E \leq$ 100 TeV) regime performed by MAGIC led to the first detection of the source in this energy range [8]. Observations in X-rays indicate a higher-than-usual state with respect to archival observations. Moreover, observations in the optical energy range performed by KVA in the subsequent months showed a decreasing flux after the period of the flare. The high state reported in all energy bands seemed to suggest a simple one-zone model for the modelling of its SED. In this scenario scthe emission region is assumed to be a spherical blob filled with a population of electrons distributed as a broken power-law, radiating energy via synchrotron emission and IC. The SED was also modelled with a two-component model, which proved to be in a better agreement with the data, as reported in [9].

2. HE and VHE gamma-ray observations

2.1 MAGIC observations and discovery

MAGIC is a stereoscopic system of two imaging Cherenkov telescopes located at an altitude of 2200 m in the Roque de los Muchachos Observatory. The telescopes are 17 m in diameter and the energy range goes from 50 GeV to 50 TeV. MAGIC telescopes performed observations of TXS 1515–273 from MJD 58541 until MJD 58547. A total of $\sim$ 8 hours was collected at a high

zenith angle, ranging from 55° to 62°, under different moonlight illumination levels. For a more detailed discussion on the MAGIC performance under moonlight the reader is addressed to [10].

The analysis of the data was performed with the standard tool for the MAGIC analysis, MARS [11]. We optimised the analysis procedure to take into account different levels of night sky background. The standard variable θ^2, which is defined as the squared angular distance of the reconstructed shower direction with respect to the source location in the camera, was used to look for any significant VHE gamma-ray excess with respect to background. The observations carried out during the flaring period led to a significant detection with a statistical significance of 7.6 σ in the VHE range. The statistical significance is estimated using the Li & Ma formula reported in [12].

The night-wise gamma-ray flux was derived for energies above 400 GeV. This energy threshold was employed to allow for a proper flux estimation for each night while still taking into account the observational conditions. The resulting light curve is shown in the top panel of Figure 3.

The data acquired during all the nights were combined to evaluate the overall spectrum, since the acquired signal was not strong enough to evaluate the spectrum for each night individually. The resulting spectrum was fitted with a power-law function. In order to reconstruct the intrinsic spectrum of the source, the observed spectrum was unfolded by the energy dispersion using the Bertero method [13] and then corrected for the extragalactic background light (EBL) absorption by adopting the Domínguez model [14].

The MAGIC spectrum obtained after the unfolding and the EBL correction between 200 GeV and 900 GeV is soft and is well-described by a simple power-law model

$$\frac{dN}{dE} = N_0 \left(\frac{E}{E_0} \right)^{\Gamma} \tag{1}$$

with photon index $\Gamma = 3.11 \pm 0.32_{\text{stat}}$, decorrelation energy $E_0 = 546\,\text{GeV}$ and normalization constant $N_0 = (1.76 \pm 0.28_{\text{stat}}) \times 10^{-11}\,\text{TeV}^{-1} \cdot \text{cm}^{-2} \cdot \text{s}^{-1}$. The unfolded spectrum is shown in Figure 1, right panel, where blue stars represent the observed spectrum and red circles the deabsorbed spectrum. The red solid line represents the best-fit power-law and the shaded area represents the systematic uncertainties of the analysis. The soft spectrum in the VHE range suggests that the high-energy bump in the SED is likely to be peaking at GeV energies.

2.2 *Fermi*-LAT data analysis

The Large Area Telescope (LAT) instrument onboard the *Fermi Gamma-Ray Space Telescope* satellite is a pair-conversion telescope with a precision converter-tracker and calorimeter that detects gamma rays from tens of MeV to hundreds of GeV.

Data from TXS 1515–273 were selected in a time window in temporal coincidence with the MAGIC observations. Events in a 12° region of interest (ROI) centered on the nominal position of the source and reconstructed energy in the 300 MeV – 500 GeV range were selected. The cuts on the quality and the zenith distance were chosen following the recommendations by the *Fermi*-LAT collaboration[1].

[1]Standard cuts on the quality were used, e.g. `'DATA_QUAL>0 && LAT_CONFIG==1'` , while a zenith distance < 90° was selected.

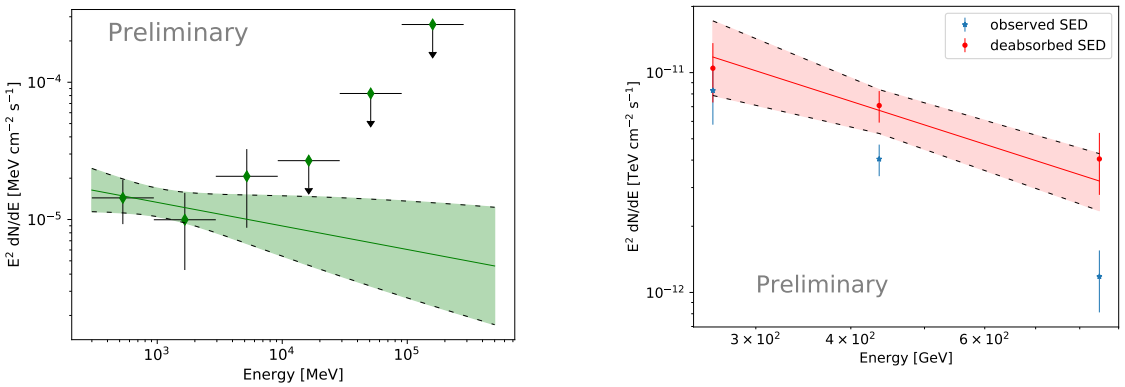

Figure 1: Right: Differential energy spectrum of TXS 1515–273 measured by the *Fermi*-LAT from MJD 58541 to MJD 58545. Data represent measurements, the solid lines the best-fit power-law model and the shaded area the statistical uncertainties of the analysis. Upper limits are shown as downward arrows. Left: Differential energy spectrum of TXS 1515–273 measured by MAGIC (blue stars) and corrected for EBL (red circles). The red solid line represents the best-fit power-law, while the red shaded area represents the systematic uncertainties of the analysis.

We performed a binned likelihood analysis[2] in a square region inscribed in the ROI selected. Data were binned in energy adopting 8 bins/decade. Spectral parameters of all the point-like sources in the ROI, which were detected within 5° from TXS 1515–273 with test statistic (TS) greater than 10, were fit in the model. The spectra of the diffuse components, both galactic and isotropic[3], were also fit. The parameters of all other sources were fixed to the published 4FGL values.

A first analysis was performed selecting a $\sim$ 4 month period around the flare, from MJD 58476 to MJD 58613. The daily binned light curve for this period is shown in Figure 2, with the MAGIC observation days highlighted in red. The reference flux from the 4FGL catalog, equals to 1.40×10^{-9} ph cm^{-2} s^{-1} is shown as a grey dotted line, clearly indicating a higher than usual state in the highlighted period.

The gamma-ray flux variability of the source in the HE band was more deeply investigated over the flare period from MJD 58541 through MJD 58548. In this period, the source was detected with TS equal to 116 which corresponds approximately to a significance of 10.8σ. The gamma-ray light curve, including both MAGIC and *Fermi*-LAT observations is shown in Figure 3.

As shown in the plot, TXS 1515–273 was found to be in a high state in the *Fermi*-LAT band during MJD 58546. However MAGIC VHE observations were not available for this night due to bad weather, as can be seen from the missing data point in the MAGIC light curve. For this reason, we decided to reduce the *Fermi*-LAT time range to MJD 58541 – 58545 so that the high flux observed on MJD 58546 would not influence the broadband SED, in order to have a smoother connection between the HE and the VHE gamma-ray observations. The resulting *Fermi*-LAT spectrum is reported in Figure 1, left panel. The spectrum is well described by a power-law model,

[2]The analysis of *Fermi*-LAT data was performed using Fermitools v1.2.1 and the `P8R3_SOURCE_V2` instrument response function.

[3]The galactic and isotropic models used were, respectively, `gll_iem_v07` and the `iso_P8R3_SOURCE_V2_v1` models.

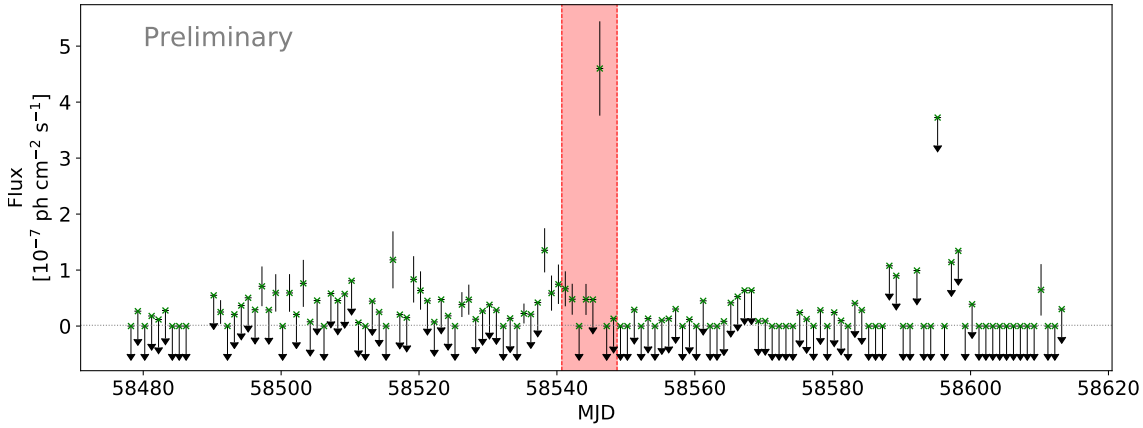

Figure 2: Gamma-ray flux light curves of TXS 1515–273 measured with the *Fermi*-LAT over a 4 month period around the flaring activity, daily binned. The red shaded area marks the period matching the MAGIC observations. 95% C.L. upper limits are shown as downward arrows for each time bin where the TS value for the source was found to be smaller than 9. The reference flux from the 4FGL catalog is shown as a grey dotted line.

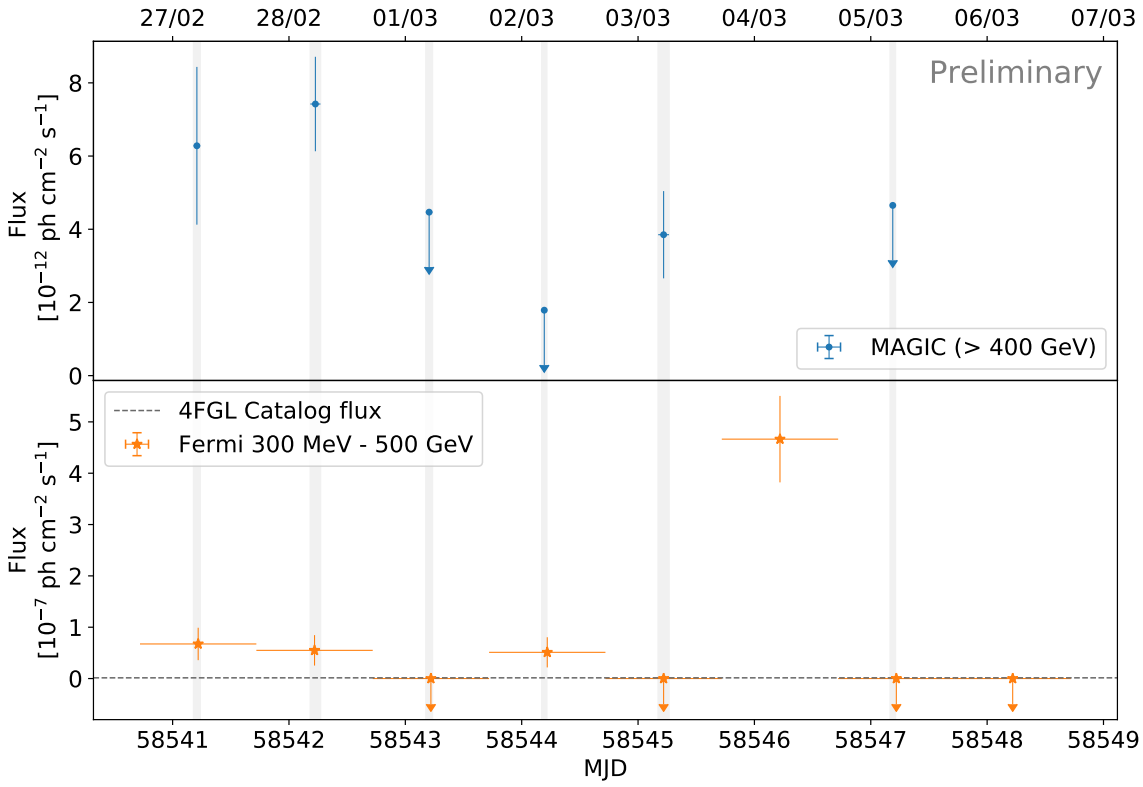

Figure 3: VHE and HE gamma-ray flux light curves of TXS 1515–273 measured with MAGIC (top, blue circles) and with the *Fermi*-LAT (bottom, orange stars) during the flaring activity, daily binned. 95% confidence upper limits are indicated as downward arrows in VHE gamma rays where the flux is compatible with zero as well as in the HE band for each time bin where the TS value for the source was found to be smaller than 9. Grey vertical bands mark the MAGIC observations.

whose spectral parameters are $N_0 = (20 \pm 7) \times 10^{-13}\,\mathrm{MeV}^{-1} \cdot \mathrm{cm}^{-2} \cdot \mathrm{s}^{-1}$, $\Gamma = 2.2 \pm 0.3$ and $f_{\mathrm{E>300\,MeV}} = (4.5 \pm 1.3) \cdot 10^{-8}\mathrm{cm}^{-2}\mathrm{s}^{-1}$ GeV, with $E_0 = 2.3$ GeV.

The spectral analysis in the time range MJD 59541 – 58548, including MJD 58546, was performed for analysis purposes. The photon index did not show any significant change between the considered time windows. Only an increase in the measured flux was observed, due to the high state observed in MJD 58546.

3. X-ray variability

The observational campaign reported here had very good coverage in the X-ray energy band. The source was observed in this energy band with the *NuSTAR* telescope, the *XMM-Newton* observatory and the *Neil Gehrels Swift* observatory. Details on the analysis in this energy band will be found in [9]. Owing to the long exposure of *XMM-Newton* and *NuSTAR*, we studied in detail the variability in the X-rays to constrain some of the parameters which we later used to model the SED.

Multiple flares were found in the light curves of *NuSTAR* and *XMM-Newton*. The flare profiles were fit using an exponential function to estimate the variability time. The time scale of the variation was found to be on the order of hours for both datasets. Such a short time scale is in agreement with the fast variability already seen in many HSPs [15]. Moreover, the rise and decay time scales of each flare are not significantly different. However, for both datasets the rise time of the high-energy light curve appears to be shorter than the rise time of the low-energy light curve, which is in agreement with a cooling dominated scenario [16].

Since the *XMM-Newton* and *NuSTAR* observations were separated by less than a day but not overlapping, and rapid variations on the time scale of hours were detected, we decided to consider the data in two separate epochs for the two observing periods in order to take into account the rapid variability in the X-rays. Therefore, we divided the dataset into two epochs, one with *XMM-Newton* and *XMM-OM* and the other with *NuSTAR* and *Swift* datasets in the X-rays and optical energy bands.

The shortest time scales found in the analysis of the flare profiles in the two epochs were then used to constrain the size of the emission region R. The upper limit on R was found to be $R \leq (5.07 \pm 0.92) \times 10^5$ cm for the *XMM-Newton* epoch and $R \leq (2.73 \pm 0.58) \times 10^5$ cm for the *NuSTAR* epoch. We assumed the Doppler factor to be $\delta = 20$, which is a typical value for VHE emitting BL Lacs.

Following the prescription described in [17] we also constrained the strength of the magnetic field of the emission region. However, since the X-ray observations are quite close in time and it is unlikely for the magnetic field strength to vary in such a short period, we combined the observations of the two epochs to constrain the magnetic field. Assuming again $\delta = 20$, the resulting magnetic field strength was found to be $B = (0.14 \pm 0.02)$ G.

4. Summary

We report here on part of a MWL analysis performed on the BL Lac object TXS 1515–273. It was found to be in a flaring state with respect to archival data in the X-ray and HE gamma-ray band, with a consequent first detection at VHE gamma-ray by MAGIC. The very good coverage in the X-rays, provided by *XMM-Newton*, *NuSTAR* and *Swift*-XRT, allowed for a detailed study of the

variability of the source in this energy band. The estimated value of the magnetic field strength, B, and the upper limits on the size of the emission region, R, were employed to model the SED of TXS 1515–273 in the two epochs. Moreover, the excellent X-ray data also allowed for a study of the synchrotron peak of the SED and the estimation of its frequency, classifying the source as HSP as it was found to have $\nu_{\rm sync} \sim 10^{15}$ Hz.

In addition the source was observed in optical and radio bands as part of the Tuorla[4] and MOJAVE[5] blazar monitoring programs. In both bands the source was little studied before these observations, but has now (after the campaign presented here) been included in regular monitoring of Tuorla[6] in optical band and TELAMON (see Kadler et al. this volume) and TANAMI [18] programs in radio band. The full analysis of the multiwavelength data set and the spectral energy distribution modelling will be presented in [9].

Acknowledgments

We acknowledge the support from the agencies and organizations listed here: https://magic.mpp.mpg.de/acknowledgments_ICRC2021 The *Fermi*-LAT Collaboration acknowledges support for LAT development, operation and data analysis from NASA and DOE (United States), CEA/Irfu and IN2P3/CNRS (France), ASI and INFN (Italy), MEXT, KEK, and JAXA (Japan), and the K.A. Wallenberg Foundation, the Swedish Research Council and the National Space Board (Sweden). Science analysis support in the operations phase from INAF (Italy) and CNES (France) is also gratefully acknowledged. This work performed in part under DOE Contract DE-AC02-76SF00515.

References

[1] A. A. Abdo et al. (2010) The Spectral Energy Distribution of Fermi Bright Blazars. ApJ, 716(1), 30-70.

[2] F. Acero et al. (2015) Fermi Large Area Telescope Third Source Catalog. ApJ Supplement, 218(2), 23.

[3] J. Lefaucheur et al. (2017) Research and characterisation of blazar candidates among the Fermi-LAT 3FGL catalogue using multivariate classifications. A&A, 602, A86.

[4] The Fermi-LAT collaboration. (2020) Fermi Large Area Telescope Fourth Source Catalog. ApJS, 247, 33.

[5] P. Goldoni et al. (2020) Optical spectroscopy of Blazars for the Cherenkov Telescope Array, arXiv:2012.05176.

[6] J. Becerra González et al. (2020) Optical spectral characterization of the the gamma-ray blazars S4 0954+65, TXS 1515-273 and RX J0812.0+0237, arXiv:2010.14532.

[4] http://users.utu.fi/kani/1m

[5] https://www.physics.purdue.edu/MOJAVE/

[6] restarting in 2021 using the 80 cm Joan Oró Telescope at Montsec Astronomical Observatory, Spain.

[7] S. Cutini (2019) Fermi-LAT detection of a GeV flare from high-synchrotron-peaked blazar TXS 1515-273. The Astronomer's Telegram, 12532.

[8] R. Mirzoyan (2019) Detection of sub-TeV gamma-ray emission from the flaring blazar TXS 1515-273 with the MAGIC telescopes. The Astronomer's Telegram, 12538.

[9] MAGIC Collaboration et al. (2021) First detection of VHE gamma-ray emission from TXS 1515–273, study of its X-ray variability and spectral energy distribution, arXiv:2107.09413, accepted in MNRAS.

[10] M.L. Ahnen et al. (2017) Performance of the MAGIC telescopes under moonlight. Astroparticle Physics, 94, 29-41.

[11] R. Zanin et al. (2013) MARS, The MAGIC Analysis and Reconstruction Software. Braz.J.Phys. 44, 5,415-608

[12] Li and Y. Ma (1983) Analysis methods for results in gamma-ray astronomy. Astrophysical Journal,272:317-324.

[13] J. Albert et al. Unfolding of differential energy spectra in the MAGIC experiment. Nuclear Instruments and Methods in Physics Research Section A, Volume 583, Issue 2-3:494-506. 2007.

[14] A. Domínguez et al. (2011) Extragalactic background light inferred from AEGIS galaxy-SED-type fractions. MNRAS, 410-4, 2556–2578.

[15] G. Bhatta et al. (2018) Hard X-ray properties of NuSTAR blazars. A& A, 619:A93.

[16] J. G. Kirk et al. (1998) Particle acceleration and synchrotron emission in blazar jets. A& A, 333:452–458.

[17] Y. H. Zhang et al. (2002) Four Years of Monitoring Blazar PKS 2155–304 with BeppoSAX: Probing the Dynamics of the Jet. ApJ, 572 762

[18] Ojha, R. et al. (2020), TANAMI VLBI Monitoring and the Doppler Crisis in the CTA Era. American Astronomical Society Meeting Abstracts, 236.

The MAGIC Collaboration

V. A. Acciari[1], S. Ansoldi[2,41], L. A. Antonelli[3], A. Arbet Engels[4], M. Artero[5], K. Asano[6], D. Baack[7], A. Babić[8], A. Baquero[9], U. Barres de Almeida[10], J. A. Barrio[9], I. Batković[11], J. Becerra González[1], W. Bednarek[12], L. Bellizzi[13], E. Bernardini[14], M. Bernardos[11], A. Berti[15], J. Besenrieder[15], W. Bhattacharyya[14], C. Bigongiari[3], A. Biland[4], O. Blanch[5], H. Bökenkamp[7], G. Bonnoli[16], Ž. Bošnjak[8], G. Busetto[11], R. Carosi[17], G. Ceribella[15], M. Cerruti[18], Y. Chai[15], A. Chilingarian[19], S. Cikota[8], S. M. Colak[5], E. Colombo[1], J. L. Contreras[9], J. Cortina[20], S. Covino[3], G. D'Amico[15,42], V. D'Elia[3], P. Da Vela[17,43], F. Dazzi[3], A. De Angelis[11], B. De Lotto[2], M. Delfino[5,44], J. Delgado[5,44], C. Delgado Mendez[20], D. Depaoli[21], F. Di Pierro[21], L. Di Venere[22], E. Do Souto Espiñeira[5], D. Dominis Prester[23], A. Donini[2], D. Dorner[24], M. Doro[11], D. Elsaesser[7], V. Fallah Ramazani[25,45], A. Fattorini[7], M. V. Fonseca[9], L. Font[26], C. Fruck[15], S. Fukami[6], Y. Fukazawa[27], R. J. García López[1], M. Garczarczyk[14], S. Gasparyan[28], M. Gaug[26], N. Giglietto[22], F. Giordano[22], P. Gliwny[12], N. Godinović[29], J. G. Green[3], D. Green[15], D. Hadasch[6], A. Hahn[15], L. Heckmann[15], J. Herrera[1], J. Hoang[9,46], D. Hrupec[30], M. Hütten[15], T. Inada[6], K. Ishio[12], Y. Iwamura[6], I. Jiménez Martínez[20], J. Jormanainen[25], L. Jouvin[5], M. Karjalainen[1], D. Kerszberg[5], Y. Kobayashi[6], H. Kubo[31], J. Kushida[32], A. Lamastra[3], D. Lelas[29], F. Leone[3], E. Lindfors[25],

L. Linhoff[7], S. Lombardi[3], F. Longo[2,47], R. López-Coto[11], M. López-Moya[9], A. López-Oramas[1], S. Loporchio[22], B. Machado de Oliveira Fraga[10], C. Maggio[26], P. Majumdar[33], M. Makariev[34], M. Mallamaci[11], G. Maneva[34], M. Manganaro[23], K. Mannheim[24], L. Maraschi[3], M. Mariotti[11], M. Martínez[5], D. Mazin[6,15], S. Menchiari[13], S. Mender[7], S. Mićanović[23], D. Miceli[2,49], T. Miener[9], J. M. Miranda[13], R. Mirzoyan[15], E. Molina[18], A. Moralejo[5], D. Morcuende[9], V. Moreno[26], E. Moretti[5], T. Nakamori[35], L. Nava[3], V. Neustroev[36], C. Nigro[5], K. Nilsson[25], K. Nishijima[32], K. Noda[6], S. Nozaki[31], Y. Ohtani[6], T. Oka[31], J. Otero-Santos[1], S. Paiano[3], M. Palatiello[2], D. Paneque[15], R. Paoletti[13], J. M. Paredes[18], L. Pavletić[23], P. Peñil[9], M. Persic[2,50], M. Pihet[15], P. G. Prada Moroni[17], E. Prandini[11], C. Priyadarshi[5], I. Puljak[29], W. Rhode[7], M. Ribó[18], J. Rico[5], C. Righi[3], A. Rugliancich[17], N. Sahakyan[28], T. Saito[6], S. Sakurai[6], K. Satalecka[14], F. G. Saturni[3], B. Schleicher[24], K. Schmidt[7], T. Schweizer[15], J. Sitarek[12], I. Šnidarić[37], D. Sobczynska[12], A. Spolon[11], A. Stamerra[3], J. Strišković[30], D. Strom[15], M. Strzys[6], Y. Suda[27], T. Surić[37], M. Takahashi[6], R. Takeishi[6], F. Tavecchio[3], P. Temnikov[34], T. Terzić[23], M. Teshima[15,6], L. Tosti[38], S. Truzzi[13], A. Tutone[3], S. Ubach[26], J. van Scherpenberg[15], G. Vanzo[1], M. Vazquez Acosta[1], S. Ventura[13], V. Verguilov[34], C. F. Vigorito[21], V. Vitale[39], I. Vovk[6], M. Will[15], C. Wunderlich[13], T. Yamamoto[40], and D. Zarić[29]

[1] Instituto de Astrofísica de Canarias and Dpto. de Astrofísica, Universidad de La Laguna, E-38200, La Laguna, Tenerife, Spain [2] Università di Udine and INFN Trieste, I-33100 Udine, Italy [3] National Institute for Astrophysics (INAF), I-00136 Rome, Italy [4] ETH Zürich, CH-8093 Zürich, Switzerland [5] Institut de Física d'Altes Energies (IFAE), The Barcelona Institute of Science and Technology (BIST), E-08193 Bellaterra (Barcelona), Spain [6] Japanese MAGIC Group: Institute for Cosmic Ray Research (ICRR), The University of Tokyo, Kashiwa, 277-8582 Chiba, Japan [7] Technische Universität Dortmund, D-44221 Dortmund, Germany [8] Croatian MAGIC Group: University of Zagreb, Faculty of Electrical Engineering and Computing (FER), 10000 Zagreb, Croatia [9] IPARCOS Institute and EMFTEL Department, Universidad Complutense de Madrid, E-28040 Madrid, Spain [10] Centro Brasileiro de Pesquisas Físicas (CBPF), 22290-180 URCA, Rio de Janeiro (RJ), Brazil [11] Università di Padova and INFN, I-35131 Padova, Italy [12] University of Lodz, Faculty of Physics and Applied Informatics, Department of Astrophysics, 90-236 Lodz, Poland [13] Università di Siena and INFN Pisa, I-53100 Siena, Italy [14] Deutsches Elektronen-Synchrotron (DESY), D-15738 Zeuthen, Germany [15] Max-Planck-Institut für Physik, D-80805 München, Germany [16] Instituto de Astrofísica de Andalucía-CSIC, Glorieta de la Astronomía s/n, 18008, Granada, Spain [17] Università di Pisa and INFN Pisa, I-56126 Pisa, Italy [18] Universitat de Barcelona, ICCUB, IEEC-UB, E-08028 Barcelona, Spain [19] Armenian MAGIC Group: A. Alikhanyan National Science Laboratory, 0036 Yerevan, Armenia [20] Centro de Investigaciones Energéticas, Medioambientales y Tecnológicas, E-28040 Madrid, Spain [21] INFN MAGIC Group: INFN Sezione di Torino and Università degli Studi di Torino, I-10125 Torino, Italy [22] INFN MAGIC Group: INFN Sezione di Bari and Dipartimento Interateneo di Fisica dell'Università e del Politecnico di Bari, I-70125 Bari, Italy [23] Croatian MAGIC Group: University of Rijeka, Department of Physics, 51000 Rijeka, Croatia [24] Universität Würzburg, D-97074 Würzburg, Germany [25] Finnish MAGIC Group: Finnish Centre for Astronomy with ESO, University of Turku, FI-20014 Turku, Finland [26] Departament de Física, and CERES-IEEC, Universitat Autònoma de Barcelona, E-08193 Bellaterra, Spain [27] Japanese MAGIC Group: Physics Program, Graduate School of Advanced Science and Engineering, Hiroshima University, 739-8526 Hiroshima, Japan [28] Armenian MAGIC Group: ICRANet-Armenia at NAS RA, 0019 Yerevan, Armenia [29] Croatian MAGIC Group: University of Split, Faculty of Electrical Engineering, Mechanical Engineering and Naval Architecture (FESB), 21000 Split, Croatia [30] Croatian MAGIC Group: Josip Juraj Strossmayer University of Osijek, Department of Physics, 31000 Osijek, Croatia [31] Japanese MAGIC Group: Department of Physics, Kyoto University, 606-8502 Kyoto, Japan [32] Japanese MAGIC Group: Department of Physics, Tokai University, Hiratsuka, 259-1292 Kanagawa, Japan [33] Saha Institute of Nuclear Physics, HBNI, 1/AF Bidhannagar, Salt Lake, Sector-1, Kolkata 700064, India [34] Inst. for Nucl. Research and Nucl. Energy, Bulgarian Academy of Sciences, BG-1784 Sofia, Bulgaria [35] Japanese MAGIC Group: Department of Physics, Yamagata University, Yamagata 990-8560, Japan [36] Finnish MAGIC Group: Astronomy Research Unit, University of Oulu, FI-90014 Oulu, Finland [37] Croatian MAGIC Group: Ruđer Bošković Institute, 10000 Zagreb, Croatia [38] INFN MAGIC Group: INFN Sezione di Perugia, I-06123 Perugia, Italy [39] INFN MAGIC Group: INFN Roma Tor Vergata, I-00133 Roma, Italy [40] Japanese MAGIC Group: Department of Physics, Konan University, Kobe, Hyogo 658-8501, Japan [41] also at International Center for Relativistic Astrophysics (ICRA), Rome, Italy [42] now at Department for Physics and Technology, University of Bergen, NO-5020, Norway [43] now at University of Innsbruck [44] also at Port d'Informació Científica (PIC), E-08193 Bellaterra (Barcelona), Spain [45] now at Ruhr-Universität Bochum, Fakultät für Physik und Astronomie, Astronomisches Institut (AIRUB), 44801 Bochum, Germany [46] now at Department of Astronomy, University of California Berkeley, Berkeley CA 94720 [47] also at Dipartimento di Fisica, Università di Trieste, I-34127 Trieste, Italy [49] now at Laboratoire d'Annecy de Physique des Particules (LAPP), CNRS-IN2P3, 74941 Annecy Cedex, France [50] also at INAF Trieste and Dept. of Physics and Astronomy, University of Bologna, Bologna, Italy

PoS(ICRC2021)801